Mixed layer depth seasonality modulates summertime SST variability in the Southern Ocean

Earle Andre Wilson[1], David Bonan[2], Andrew Thompson[2], Natalie Armstrong[3], and Stephen Riser[4]

[1]Stanford University
[2]California Institute of Technology
[3]John Hopkins University
[4]University of Washington

November 21, 2022

Abstract

In recent years, the Southern Ocean has experienced unprecedented surface warming and sea ice loss—a stark reversal of sea ice expansion and surface cooling trends that prevailed over preceding decades. The most dramatic changes occurred in the austral spring of 2016 when Antarctic sea-ice extent (SIE) reached a record minimum as sea surface temperatures (SST) climbed to a near-record high. In late 2019, another circumpolar surface warming event spanned the Southern Ocean, albeit with no appreciable decline in Antarctic SIE. A mixed layer heat budget analysis reveals that these recent circumpolar surface warming events were triggered by a weakening of the circumpolar westerlies, which decreased northward Ekman transport and accelerated the seasonal shoaling of the mixed layer. The latter effect amplified the surface warming effect of air-sea heat fluxes during months of peak solar insolation. More generally, summertime SST across the Southern Ocean is sensitive to the timing of the springtime shoaling of the mixed layer, which is controlled by the strength and temporal variance of the circumpolar westerlies. An examination of the CESM1 large ensemble demonstrates that these recent circumpolar warming events are consistent with the internal variability associated with the Southern Annual Mode (SAM), whereby negative SAM in austral spring favors shallower mixed layers and anomalously high summertime SST. Thus, future Southern Ocean surface warming extremes will depend on the evolution of regional mixed layer depths and interannual SAM variability.

Mixed layer depth seasonality modulates summertime SST variability in the Southern Ocean

Earle A. Wilson,[a] David B. Bonan,[b] Andrew F. Thompson,[b] Natalie Armstrong,[c] and Stephen C. Riser[d]

[a] *Department of Earth System Science, Stanford University, Stanford, CA, USA*

[b] *Environmental Science and Engineering, California Institute of Technology, Pasadena, CA, USA*

[c] *Department of Environmental Health and Engineering, Johns Hopkins University, Baltimore, MD, USA*

[d] *School of Oceanography, University of Washington, Seattle, WA, USA*

Corresponding author: Earle A. Wilson, earlew@stanford.edu

ABSTRACT: In recent years, the Southern Ocean has experienced unprecedented surface warming and sea ice loss—a stark reversal of sea ice expansion and surface cooling trends that prevailed over preceding decades. The most dramatic changes occurred in the austral spring of 2016 when Antarctic sea-ice extent (SIE) reached a record minimum as sea surface temperatures (SST) climbed to a near-record high. In late 2019, another circumpolar surface warming event spanned the Southern Ocean, albeit with no appreciable decline in Antarctic SIE. A mixed layer heat budget analysis reveals that these recent circumpolar surface warming events were triggered by a weakening of the circumpolar westerlies, which decreased northward Ekman transport and accelerated the seasonal shoaling of the mixed layer. The latter effect amplified the surface warming effect of air-sea heat fluxes during months of peak solar insolation. More generally, summertime SST across the Southern Ocean is sensitive to the timing of the springtime shoaling of the mixed layer, which is controlled by the strength and temporal variance of the circumpolar westerlies. An examination of the CESM1 large ensemble demonstrates that these recent circumpolar warming events are consistent with the internal variability associated with the Southern Annual Mode (SAM), whereby negative SAM in austral spring favors shallower mixed layers and anomalously high summertime SST. Thus, future Southern Ocean surface warming extremes will depend on the evolution of regional mixed layer depths and interannual SAM variability.

SIGNIFICANCE STATEMENT: This study examines the physical mechanisms that can produce abrupt and extreme surface warming across the Southern Ocean. Using the unprecedented late 2016 and 2019 Southern Ocean warming events as case studies, we demonstrate that the strength of the circumpolar westerlies in the spring strongly modulates regional sea surface temperatures (SSTs) in the summer. Weak circumpolar winds reduce the northward Ekman transport of cool subpolar waters and cause the mixed layer to shoal more rapidly in the spring. The latter effect traps more heat near the surface as the total air-sea heat flux to the ocean approaches its annual maximum. Further, we demonstrate that the unprecedented 2016 and 2019 Southern Ocean warming events are consistent with the internal variability associated with the Southern Annular Mode (SAM). These results suggest future Southern Ocean surface warming extremes will depend on the evolution of regional mixed layer depths and interannual SAM variability.

1. Introduction

The Southern Ocean has experienced exceptional sea ice decline and surface warming in recent years (Figure 1). During the austral spring of 2016, Antarctic sea ice retreated at an unusually rapid rate before reaching a record-low extent the following summer (Turner et al. 2017; Parkinson 2019; Eayrs et al. 2021). This anomalous sea ice decline coincided with widespread surface warming that extended beyond the Antarctic sea ice zone and culminated in record-high summertime sea surface temperatures (SSTs) (Stuecker et al. 2017; Meehl et al. 2019, Figure 1a). While Southern Ocean SSTs returned to normal after a few months, Antarctic sea-ice extent (SIE) remained exceptionally low over the next three years. In late 2019, the Southern Ocean experienced another abrupt circumpolar surface warming event of similar magnitude and spatial extent as the anomalous warming of late 2016, but there was no corresponding decline in Antarctic SIE (Figure 1b).

The extent to which these recent warming and sea ice loss anomalies reflect a shift in the Southern Ocean climate or transient manifestations of internal variability remains unclear. Over the preceding decades, the Southern Ocean experienced robust sea ice expansion and surface cooling that were near circumpolar in extent (Yuan and Martinson 2000; Cavalieri et al. 2003; Simmonds 2015). The underlying drivers responsible for these longer timescale trends are uncertain; possible mechanisms include the strengthening of the circumpolar westerlies (Fan et al. 2014; Kostov et al. 2017), increases in surface freshwater fluxes and stratification (Bintanja et al. 2013; Purich et al.

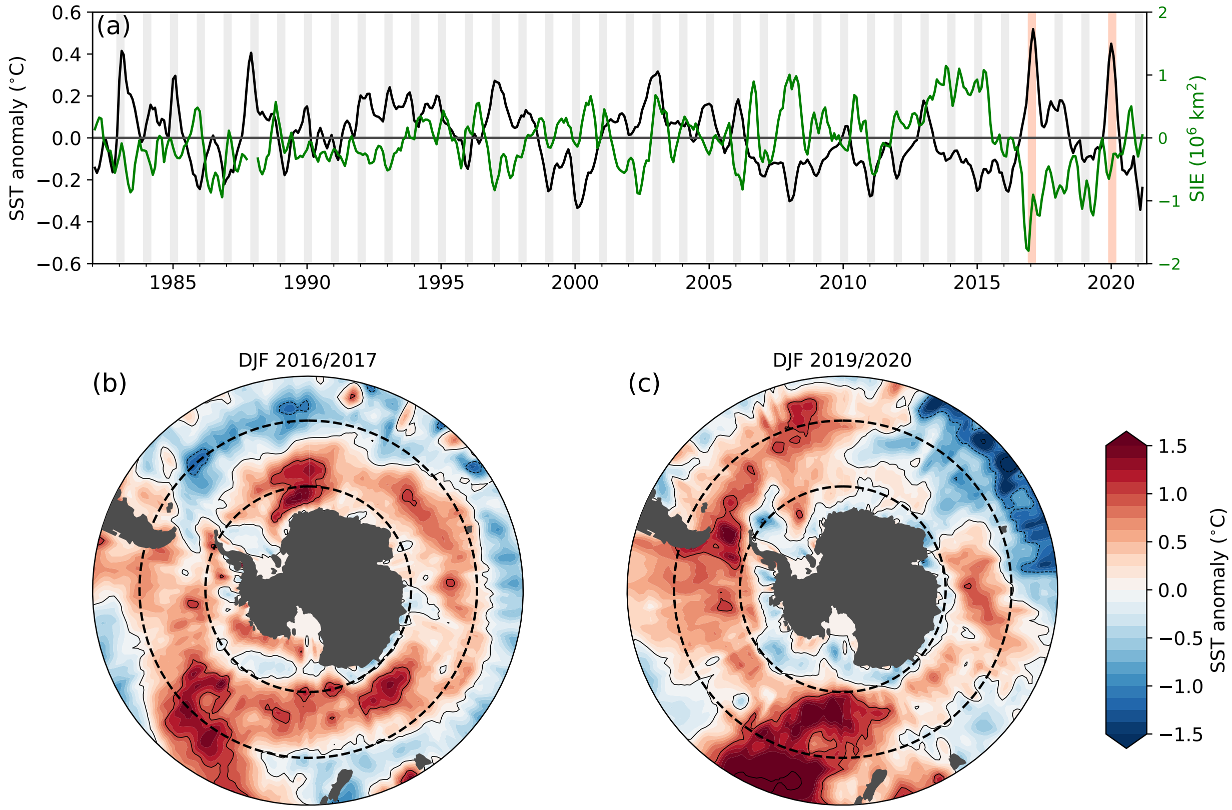

FIG. 1. (a) Temporal evolution of anomalous SST (black) and Antarctic SIE (green) in the Southern Ocean. (b, c) Seasonally averaged maps of anomalous SST during December–February (DJF) of 2016/2017 and 2019/2020. In (a), the vertical gray bars highlight austral summer (December–February). Dashed lines in (b) and (c) highlight 50°S–65°S, the latitudes over which the SST anomalies are spatially averaged in (a). Each time series has been smoothed with a 3-month rolling average.

2018; Haumann et al. 2020), atmospheric teleconnections from the tropical Pacific (Meehl et al. 2016; Li et al. 2021; Chung et al. 2022), and internal climate variability associated with Weddell Sea deep convection (Zhang et al. 2019). While it is certain that ongoing greenhouse emissions will eventually lead to sustained warming and sea ice loss across the Southern Ocean (Ferreira et al. 2015; Armour et al. 2016; Kostov et al. 2017), the timescale over which an anthropogenic signal will emerge above the noise of internal variability is poorly constrained (Doddridge et al. 2019; Rackow et al. 2022).

Previous studies suggest that the anomalous decline in Antarctic SIE that began in 2016 was due to multiple mechanisms operating over various timescales. This sea ice loss event has been linked to anomalous variations in the Southern Annular Mode (SAM), El Niño–Southern Oscillation (ENSO), and Indian Ocean Dipole (IOD), which collectively weakened the circumpolar westerly jet and facilitated anomalous poleward advection of warm subtropical air into the subpolar region (Stuecker et al. 2017; Schlosser et al. 2018; Wang et al. 2019; Purich and England 2019). These mechanisms are distinct from the slower process of enhanced upwelling of warm Circumpolar Deep Water (CDW) that is expected to drive Southern Ocean sea ice loss and surface warming over the next century (Bitz and Polvani 2012; Ferreira et al. 2015). However, there is evidence that the gradual build-up of subsurface heat in the seasonal sea ice zone may have preconditioned some areas of the Southern Ocean for an unusually rapid springtime retreat of Antarctic sea ice (Meehl et al. 2019; Campbell et al. 2019).

It is likely that the mechanisms responsible for the recent decline in Antarctic sea ice are related but distinct from those that led to the recent circumpolar surface warming events. Though the 2016 surface warming coincided with a steep loss in Antarctic sea ice, this was not the case in late 2019 (Figure 1a). Furthermore, previous circumpolar surface warming events, such as those that occurred during the austral spring and summers of 1982/1983 and 1987/1988, were not accompanied by an appreciable decrease in Antarctic SIE (Figure 1a). As with the late 2016 and 2019 warming events, other prominent circumpolar warming events extended beyond the seasonal sea ice zone. Though previous studies have established links between Southern Ocean SST anomalies and the variance of SAM and ENSO (Sen Gupta and England 2006; Sallée et al. 2010; Ciasto and England 2011; Ding et al. 2012), there is no clear relationship between the intensity of SAM or ENSO phases and the magnitude of Southern Ocean SST anomalies. Thus, the particular set of circumstances that facilitated the extraordinary summertime SST anomalies in 2016/2017 and 2019/2020 remain unclear. Since these surface warming events occur in spring and summer, they also provide a glimpse of the maximum SSTs that may occur across the Southern Ocean. Critically, circumpolar warming events may provide the basis for marine heatwaves (MHWs), which are more localized SST extremes that can lead to sharp declines in biodiversity and the collapse of ecosystems (Hobday et al. 2016; Frölicher et al. 2018; Holbrook et al. 2019; Smale et al. 2019; Oliver et al. 2021). Therefore, understanding the mechanisms that may lead to surface warming extremes is an essential step toward characterizing and predicting ecological sustainability in the Southern Ocean.

The primary purpose of this work is to elucidate the large-scale atmospheric and oceanic processes that give rise to extreme and abrupt circumpolar surface warming across the Southern Ocean. This work builds on previous analyses that have examined the seasonal evolution of Southern Ocean mixed layer temperature (MLT) (Dong et al. 2007, 2008; Tamsitt et al. 2016; Pellichero et al. 2017) by focusing on processes that can lead to severe surface warming. Likewise, our analysis extends previous work that has explored the Southern Ocean response to SAM and ENSO (Sen Gupta and England 2006; Sallée et al. 2010; Ciasto and England 2011) by explicitly examining how the seasonal phasing of these modes of climate variability can produce extreme summertime SSTs. In doing so, we assess the extent to which recent circumpolar surface warming anomalies can be explained by internal variability. A key result of this analysis is that variations in the seasonal phasing of mixed layer depth (MLD) and solar insolation during austral spring are a major source of interannual variability in Southern Ocean summertime SST. In particular, a sustained period of negative SAM in late austral spring, similar to what occurred in late 2016 and 2019, provides favorable conditions for abrupt and widespread surface warming anomalies across the Southern Ocean.

2. Data and Methods

a. Observations and reanalyses

Monthly SST data were obtained from the NOAA Optimum Interpolation (OI) SST V2 product (Reynolds et al. 2002), while subsurface temperature and salinity variability are assessed from the Argo-based Roemmich-Gilson climatology (Roemmich and Gilson 2009). Estimates of Antarctic sea ice concentration (SIC) were retrieved from the NOAA/NSIDC Climate Data Record (CDR) of SIC (Meier et al. 2013). SIE is defined as the area over which SIC is greater than 15%. Estimates of surface wind stress, sea level pressure, and air-sea heat fluxes were sourced from the ECMWF monthly ERA5 global atmospheric reanalysis (Hersbach et al. 2020). The reanalysis estimates were regridded from a 0.25° by 0.25° horizontal grid to a coarser 1° by 1° horizontal grid using a bi-linear interpolation scheme, consistent with the RG Argo and the NOAA OI SST data products.

While the SST data and atmospheric reanalysis products are analyzed for 1982–2020, the mixed layer heat budget analysis is carried out for the 2004–2020 period when subsurface Argo data are available. The depth of the mixed layer is defined using a density threshold of 0.03 kg m^{-3} (de

Boyer Montégut et al. 2004). The SAM index is defined as the zonal-mean sea level pressure difference between 65°S and 40°S (Marshall 2003). ENSO variability is quantified using the Niño3.4 index, which describes the area-averaged SST anomaly between 170°W–120°W and 5°S–5°N. The SAM and Niño3.4 indices are normalized by their respective standard deviations. Anomalies are computed relative to a monthly averaged climatology. For the SST and reanalysis data, the climatological reference period is 1982–2015, while for the Argo data, the climatological reference period is 2004–2015.

To contextualize recent abrupt circumpolar warming events, observations are compared with output from the Community Earth System Model Version 1 Large Ensemble (CESM1-LE) (Kay et al. 2015). The CESM1-LE is a state-of-the-art fully coupled, 1° horizontal resolution 40-member initial condition ensemble, where each ensemble member is subjected to identical historical and RCP8.5 external forcing scenarios. However, each member differs slightly in the initial atmospheric state, producing a representation of internal variability across ensemble members, in the presence of forced climate change. We focus on the 1980–2020 period that overlaps with the modern satellite record.

b. Southern Ocean mixed layer heat budget

Physical controls on Southern Ocean SST are evaluated using a mixed layer heat budget. In this study, MLT and SST are assumed to be equivalent. The heat budget is constructed for the mostly ice-free latitude band of 50°–65°S, which envelops the core of the circumpolar westerly jet and much of the Antarctic Circumpolar Current (ACC). Importantly, this is the latitudinal band over which zonally averaged SST anomalies are cool (warm) in response to a positive (negative) SAM phase (Sen Gupta and England 2006). Further north, between 30°S–50°S, the SST response to SAM is reversed. This analysis focuses on the 50°–65°S circumpolar band, over which the anomalous warming events of late 2016 and 2019 were most apparent (see Figure 1b-c).

As demonstrated by Dong et al. (2007), domain-averaged variations in MLT T_m across the circumpolar channel is primarily governed by heating due to air-sea fluxes, northward Ekman transport, and wind-driven entrainment. This balance is given by

$$\frac{1}{A_s}\iint \frac{\partial T_m}{\partial t}\,\mathrm{d}A \approx \frac{1}{A_s}\iint \left(\frac{Q_{ao}}{\rho_0\, c_w\, h_m} - v_{Ek}\frac{\partial T_m}{\partial y} - w_{ent}\frac{\Delta T}{h_m}\right)\mathrm{d}A, \tag{1}$$

$$\frac{1}{A_s}\iint \dot{T}_m\,\mathrm{d}A \approx \frac{1}{A_s}\iint \left(\dot{T}_{ao} - \dot{T}_{Ek} - \dot{T}_{ent}\right)\mathrm{d}A, \tag{2}$$

$$\dot{\overline{T}}_m \approx \dot{\overline{T}}_{ao} - \dot{\overline{T}}_{Ek} - \dot{\overline{T}}_{ent}, \tag{3}$$

where Q_{ao} is the net air-sea heat flux comprised of the sum of radiative and turbulent heat fluxes, v_{Ek} is the meridional Ekman velocity, ΔT is the temperature difference between the mixed layer and just below the mixed layer, h_m is the mixed layer depth, $w_{ent} = \dot{h}_m$ is the entrainment rate, and A_s is the surface area of the circumpolar control volume. The meridional Ekman velocity is given by $v_{Ek} = \tau^x/(\rho_0\, f\, h_m)$, where τ^x is the zonal component of the surface wind stress, $\rho_0 = 1025$ kg m^{-3} is a reference seawater density, and $f \approx 10^{-4}$ s^{-1} is the Coriolis parameter. Following the procedure outlined in Dong et al. (2007), Q_{ao} is modified slightly to account for the fraction of shortwave radiation that is transmitted through the base of the mixed layer.

Equation (3) is valid when evaluating the heat balance over the entire circumpolar channel. Over smaller spatial scales, geostrophic transport and eddy mixing, which are neglected in this framework, have leading-order impacts on surface temperature variability (Tamsitt et al. 2016; du Plessis et al. 2022; Gao et al. 2022). It is also assumed that meridional eddy fluxes across the northern and southern boundaries of the control volume make small contributions to the domain-averaged MLT tendency $\dot{\overline{T}}_m$ on monthly timescales. Though it is relatively straight-forward to evaluate $\dot{\overline{T}}_{ao}$ and $\dot{\overline{T}}_{Ek}$ from Argo data and atmospheric reanalysis, T_{ent} presents a greater challenge since it is influenced by sub-monthly variations in h_m that are not well-resolved by the current Argo observing array (Carranza and Gille 2015). Therefore, the effect of vertical entrainment is estimated from the residual of the other heat budget terms.

3. Results

a. Climate conditions during recent circumpolar warming events

During the austral spring of 2016 and 2019, the domain-averaged surface buoyancy fluxes across the Southern Ocean were not consistently different from the climatological mean (Figure 2a).

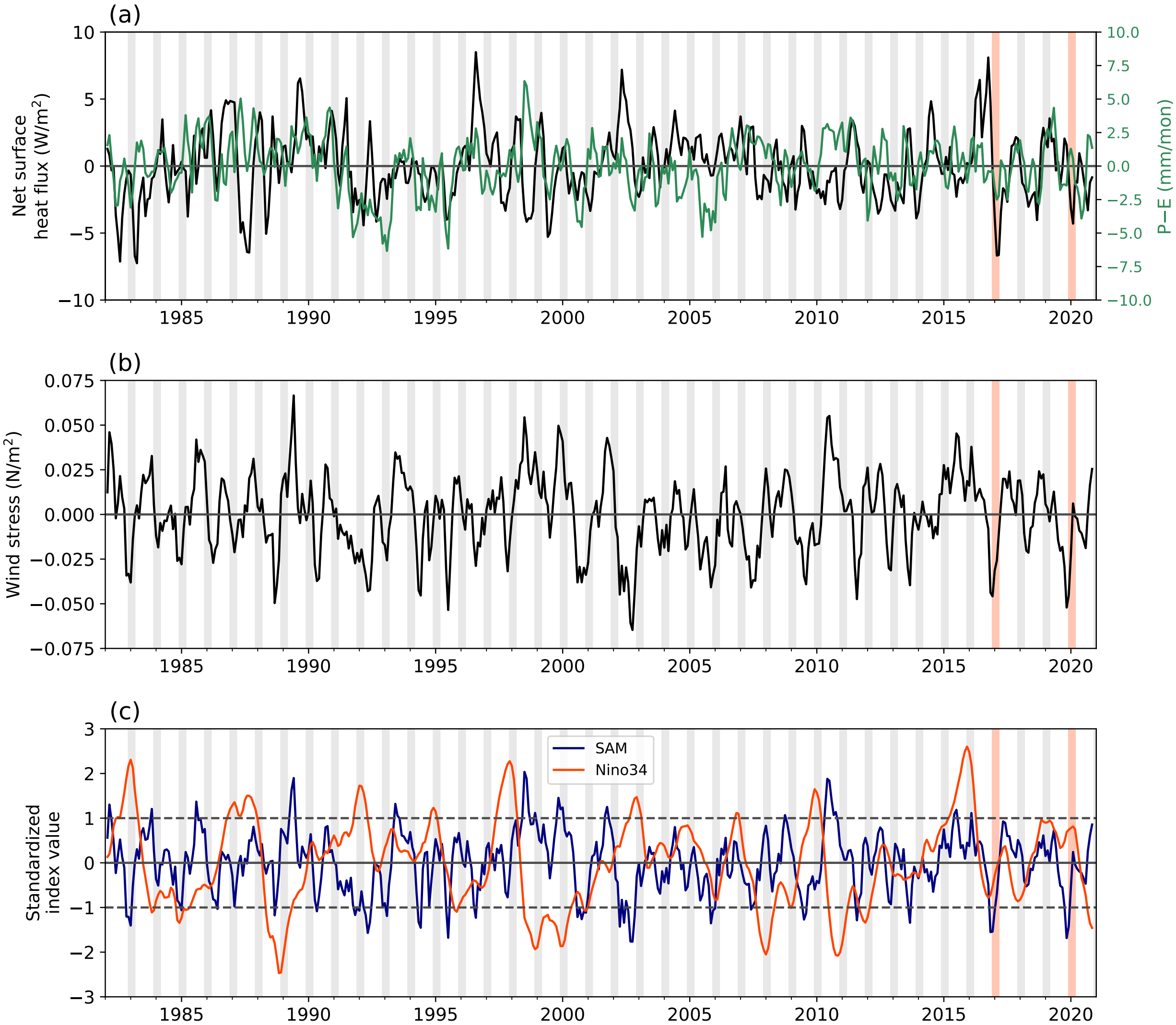

FIG. 2. (a) Domain-averaged net surface heat flux anomalies (black) and precipitation minus evaporation anomalies (P–E, green) across 50°S–65°S. Positive air-sea heat fluxes signify ocean heat gain. (b) As in (a) but showing zonal wind stress anomalies. (c) Temporal evolution of the SAM (blue) and the Nino3.4 indices (orange). Vertical gray bars highlight austral summer (December–February). The linear trend has been removed from each time series, and temporal variations are smoothed using a 3-month rolling average.

Though the late 2016 warming event followed unusually warm winter and spring, this was not the case in 2019. Additionally, the spatial patterns of anomalous air-sea fluxes were not consistent with the patterns of anomalous warming during both circumpolar warming events (Figure 3). While in some instances, patterns of anomalously high air-sea heating and mixed layer warming overlapped,

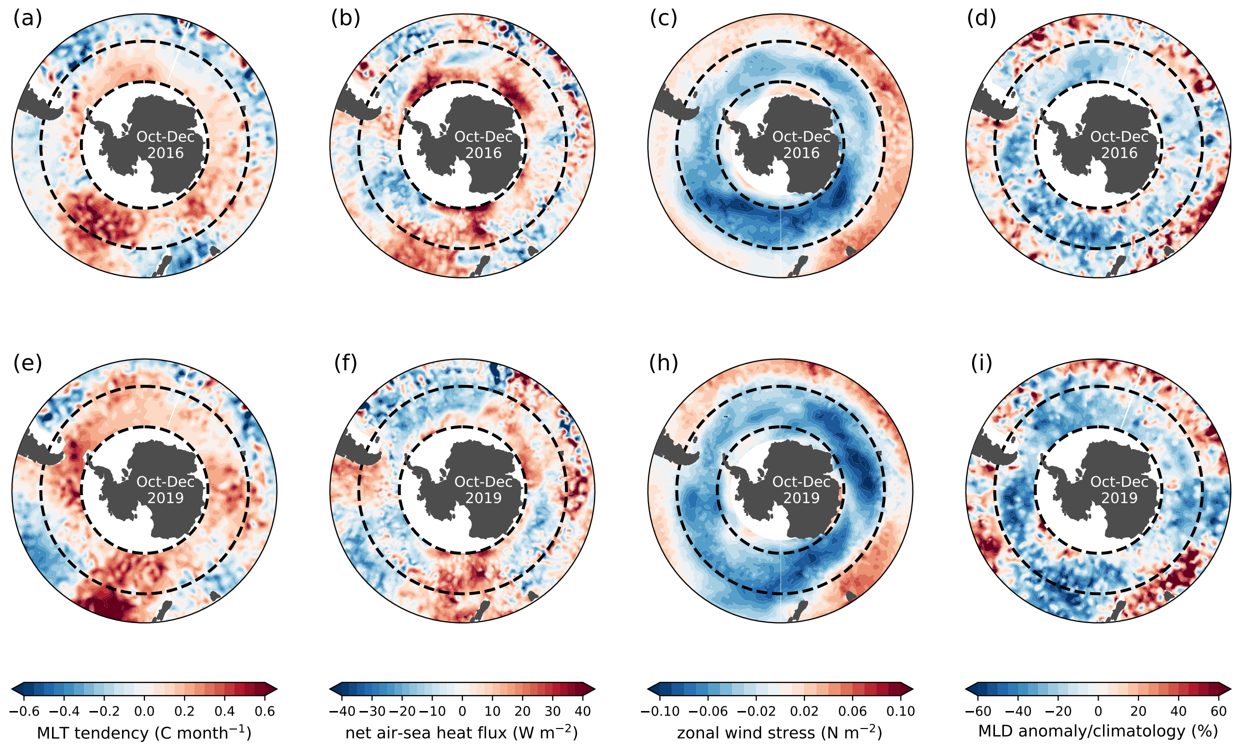

FIG. 3. Southern Ocean surface conditions during October–December of 2016 (top row) and 2019 (bottom row): (a, e) MLT tendency anomalies, (b, f) Net air-sea heat flux anomalies, (c, h) zonal wind stress anomalies, and (d, i) MLD anomalies as percentages of the monthly climatological means. Black dashed lines outline the circumpolar channel (50°S–65°S over which the mixed layer heat budget is evaluated.

this was often not the case. For example, during October–December of 2019, air-sea heat fluxes across the southern Atlantic favored anomalous surface cooling while the mixed layer warmed at an accelerated rate (Figure 3e,f). Thus, the recent circumpolar warming events cannot be directly attributed to anomalous air-sea heat fluxes.

On the other hand, circumpolar westerlies were extraordinarily weak in late 2016 and 2019, with zonally averaged surface wind stress anomalies exceeding −0.04 N m^{-2} (Figure 2b)—a $\sim$ 30% reduction relative to the climatological mean. During both warming events, the collapse of the surface westerlies spanned all longitudes (Figure 3 c, h). Concurrently, there was widespread anomalous MLD shoaling across the Southern Ocean (Figure 3d,f). The anomalous shoaling was most striking in late 2019 when the MLD across the circumpolar channel was, on average, roughly

20% shallower than usual. The late 2016 and 2019 anomalous shoaling events did not coincide with increased surface heat or freshwater fluxes (Figure 2a).

Consistent with the strong reduction in circumpolar westerly winds, SAM was in an exceptionally negative phase during both circumpolar warming events. In both cases, the SAM index was roughly 1.5 standard deviations below its annual mean value (Figure 2b). ENSO was in a relatively neutral state during these periods, tending towards its La Niña and El Nño phases during the austral spring of 2016 and 2019, respectively.

b. Drivers of anomalous mixed layer warming in late 2016 and 2019

Evaluating the circumpolar mixed layer heat budget (Equation 3) reveals that the heating anomalies associated with air-sea heat fluxes $\dot{\overline{T}}_{ao}$ and northward Ekman transport $\dot{\overline{T}}_{Ek}$ were the primary drivers of the anomalous surface warming in late 2016 and 2019 (Figure 4). In late 2016, $\dot{\overline{T}}_{Ek}$ anomalies peaked at roughly 0.08 °C month^{-1}, which was slightly less than the overall mixed layer warming of 0.1 °C month^{-1} (Figure 4b). In late 2019, anomalies in $\dot{\overline{T}}_{Ek}$ accounted for roughly half of the observed mixed layer warming. The decrease in Ekman-driven cooling is consistent with the anomalously weak zonal wind stress during these periods (Figure 3c,h). The enhancement of $\dot{\overline{T}}_{ao}$ was largely due to anomalous MLD shoaling. Thus, even though air-sea heat fluxes were not substantially different from the climatological mean during the warming events, their effect on MLT was greatly amplified.

Estimating $\dot{\overline{T}}_{ent}$ as a residual of Equation (3) suggests that entrainment-driven mixed layer cooling was enhanced during late 2016 and 2019 (Figure 4b). This implied amplification of $\dot{\overline{T}}_{ent}$ under weaker surface winds reveals a complex interplay between wind-driven mixing, MLD, and the variance of surface winds. Since $\dot{\overline{T}}_{ent}$ is dependent on MLD and the temperature gradient below the mixed layer (Eq. 3), this term does not necessarily scale with the amplitude of the surface wind stress. Moreover, the temperature of a shallower mixed layer will be more sensitive to the mixing generated by episodic storms and strong wind events. Nevertheless, without direct estimates of entrainment-driving mixing, the contribution of $\dot{\overline{T}}_{ent}$ is not well constrained.

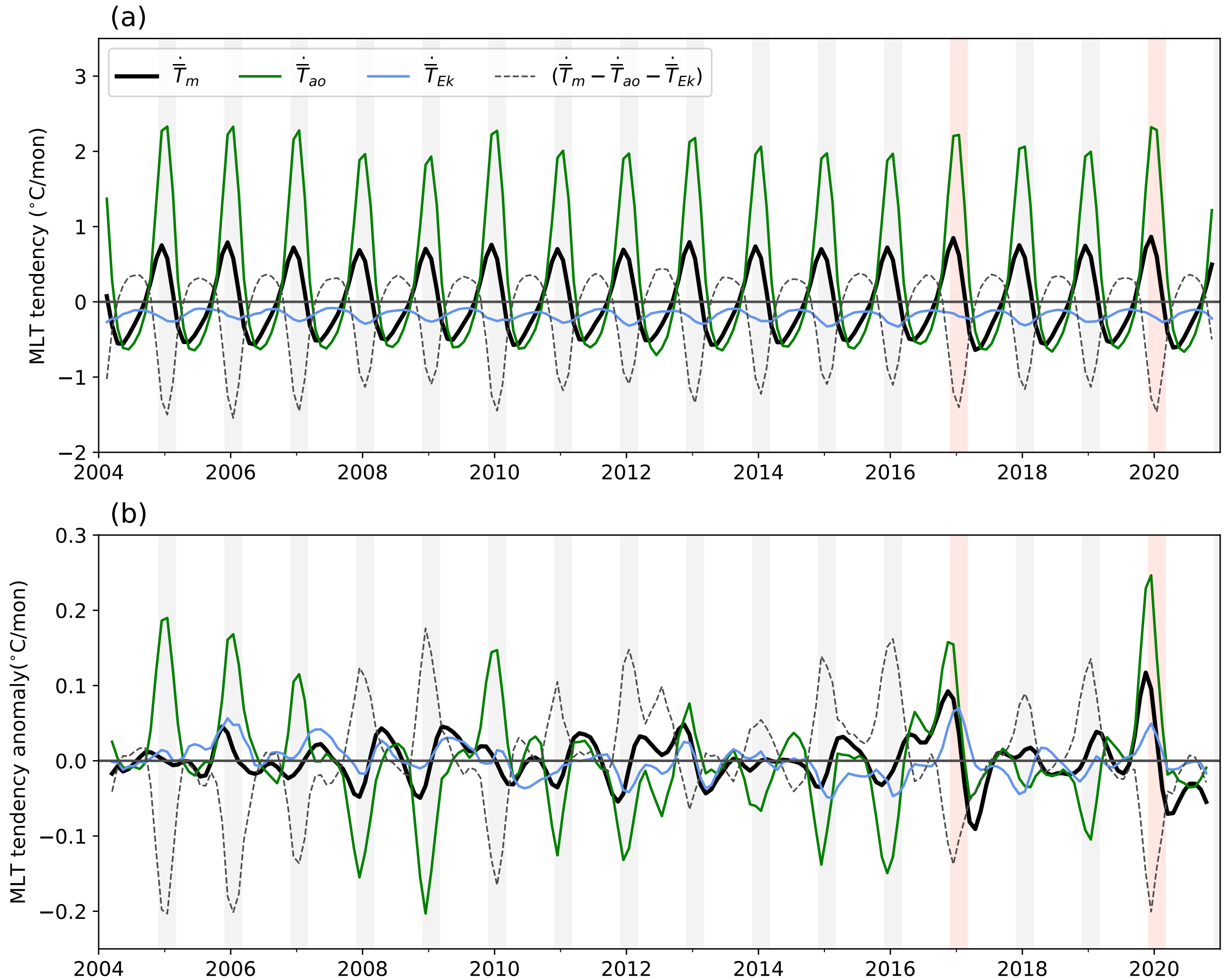

FIG. 4. Evolution of the Southern Ocean mixed layer heat budget, described by Eq. (3). (a) Monthly tendencies in MLT (black) due to air-sea heat fluxes (green) and meridional Ekman transport (blue). The gray dashed line represents the residual of the heat budget ($\dot{\overline{T}}_m - \dot{\overline{T}}_{ao} - \dot{\overline{T}}_{Ek}$), which is interpreted as the component due to entrainment. (b) As in (a) but after removing the monthly climatology. Gray vertical bars highlight December–February.

c. The seasonal phasing of mixed layer depth and air-sea heat fluxes

The seasonal evolution of $\dot{\overline{T}}_m$ is re-examined in the phase-space defined by h_m and Q_{ao} (Figure 5). Since the seasonal variation of τ^x is small compared to that of MLD and Q_{ao}, we focus on the sum of the mixed layer warming due to northward Ekman transport and air-sea heat fluxes, $\dot{\overline{T}}_{ao+Ek} \equiv \dot{\overline{T}}_{ao} + \dot{\overline{T}}_{Ek}$, assuming a constant surface wind stress of $\tau^x = 0.15$ N m^{-2}. During the cooling season (March–September), $\dot{\overline{T}}_{ao}$ and $\dot{\overline{T}}_{Ek}$ combine to cool the relatively deep mixed layer

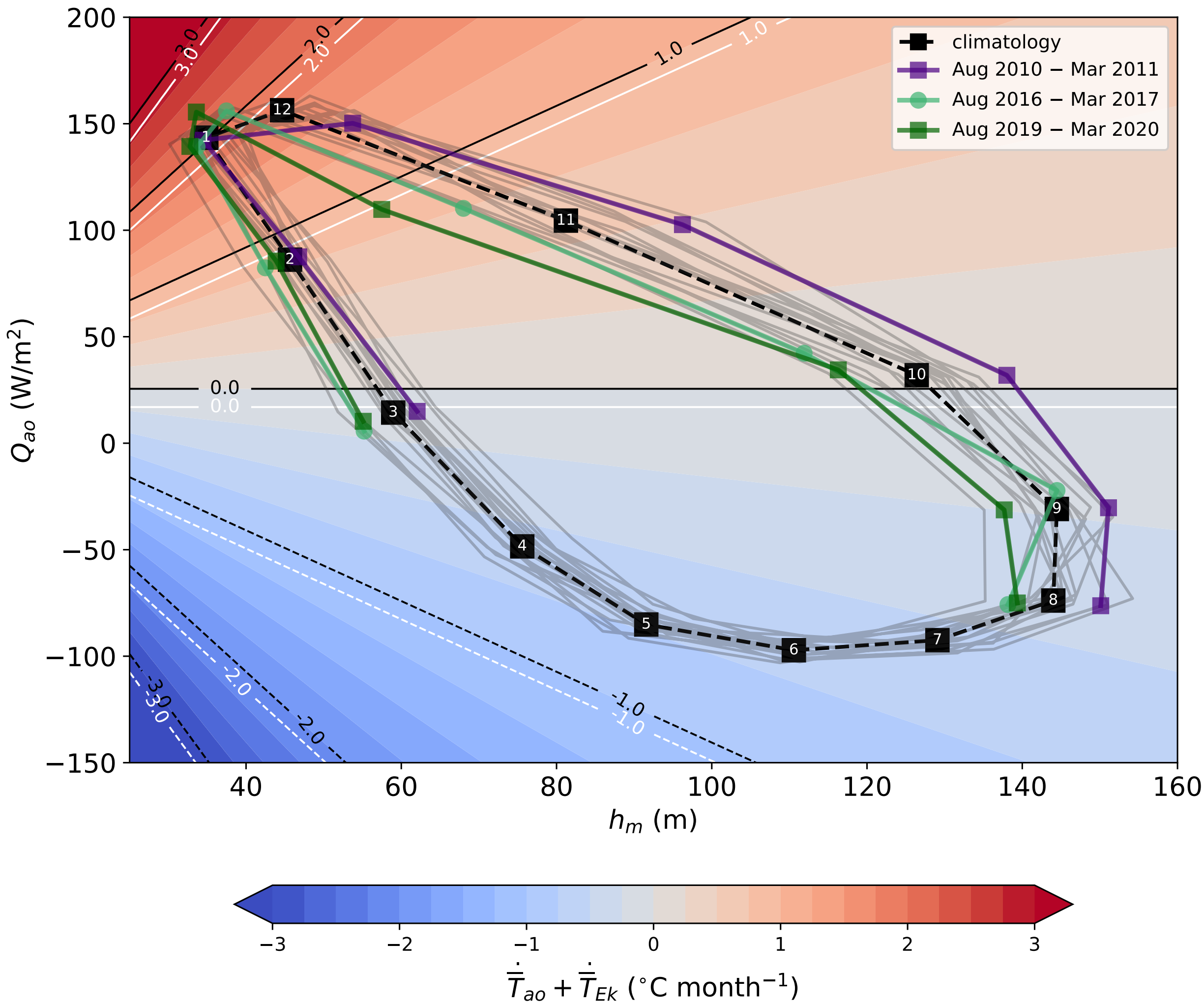

Fig. 5. Phase diagram showing the relationship between seasonal variations in mixed layer depth h_m, air-sea heat fluxes Q_{ao}, and mixed layer temperature tendency due to the sum of air-sea heating $\dot{\overline{T}}_{ao}$ and Ekman transport $\dot{\overline{T}}_{Ek}$ (contours and shading). Gray lines represent seasonal trajectories from 2004–2020, while the dashed black line represents the climatological mean. For the latter, the numbering of the black squares signifies the calendar month. The purple and green lines highlight trajectories between August–March for 2015/2016, 2016/2017, and 2019/2020, respectively. For the background shading and black contours, the heating associated with northward Ekman transport $\dot{\overline{T}}_{Ek}$ is computed assuming a typical value of $\tau^x = 0.15$ N m^{-2}. White contours show $\dot{\overline{T}}_{ao} + \dot{\overline{T}}_{Ek}$ for the case where $\tau^x = 0.1$ N m^{-2}.

at a peak rate of approximately 0.75°C month^{-1}. During the warming season (October–February), $\dot{\overline{T}}_{ao+Ek}$ provides a surface warming that reaches a maximum of ~2°C month^{-1} between January and February. The seasonal asymmetry of $\dot{\overline{T}}_{ao+Ek}$ arises from the nonlinear dependence of $\dot{\overline{T}}_{ao}$ on h_m.

As h_m approaches its summertime minimum, $\dot{\overline{T}}_{ao+Ek}$ becomes increasingly sensitive to variations in h_m and Q_{ao}, with $\dot{\overline{T}}_m$ being more sensitive to periods of anomalous mixed layer shoaling than anomalous deepening. The effect of $\dot{\overline{T}}_{Ek}$ may be discerned by the offset in the position of the $\dot{\overline{T}}_{ao+Ek} = 0$ contour in Figure 5. In the limit of no surface heating $Q_{ao} \to 0$, only northward Ekman transport contributes to heating.

In the phase-space defined by h_m and Q_{ao}, the impact of the extraordinary MLD shoaling in late 2016 and 2019 is immediately evident. During these anomalous warming periods (green lines in Figure 5), the Southern Ocean mixed layer followed a relatively shallow trajectory in the Q_{ao}–h_m phase space, which accelerated the springtime warming of the mixed layer. In most years, Q_{ao} reaches a maximum amplitude of ~150 W m^{-2} in December, one month before h_m reaches its minimum value of ~40 m. In late 2016 and 2019, the seasonal h_m minimum occurred approximately one month earlier than usual, coinciding with maximal air-sea heat fluxes. This shoaling-induced mixed layer warming anomaly was most apparent in November of 2019 when h_m was 20–30 m shallower than the climatological mean—a record low for the Argo period. The enhanced mixed layer warming due to $\dot{\overline{T}}_{ao}$ is augmented by a reduction in the cooling provided by $\dot{\overline{T}}_{Ek}$, which equates to a downward translation of the $\dot{\overline{T}}_{ao+Ek}$ pattern in Figure 5. The accelerated mixed layer warming of late 2016 and 2019, which occurred during strong negative SAM events, is contrasted with the more gradual warming that occurred in late 2010 (purple line in Figure 5), a period characterized by positive SAM conditions (Figure 2b,c). In the latter scenario, the anomalously deep Southern Ocean mixed layer warmed at a relatively slow rate, leading to anomalously cool summertime surface temperatures (Figure 1a).

d. Sensitivity of mixed layer warming to the timing of surface wind anomalies

The preceding analyses suggest that anomalous mixed layer shoaling and warming during the austral spring of 2016 and 2019 were initiated by a weakening of the circumpolar westerlies. To quantify the springtime sensitivity of MLD and MLT to surface wind variability, a set of idealized simulations were conducted using a one-dimensional ocean mixing model (Appendix A1). The Kraus-Turner mixed layer model was forced with idealized surface fluxes of buoyancy and momentum that mimic observations across 50°S–65°S during October and February (late spring through summer). For the wind stress forcing, we employ synthetic surface winds that are

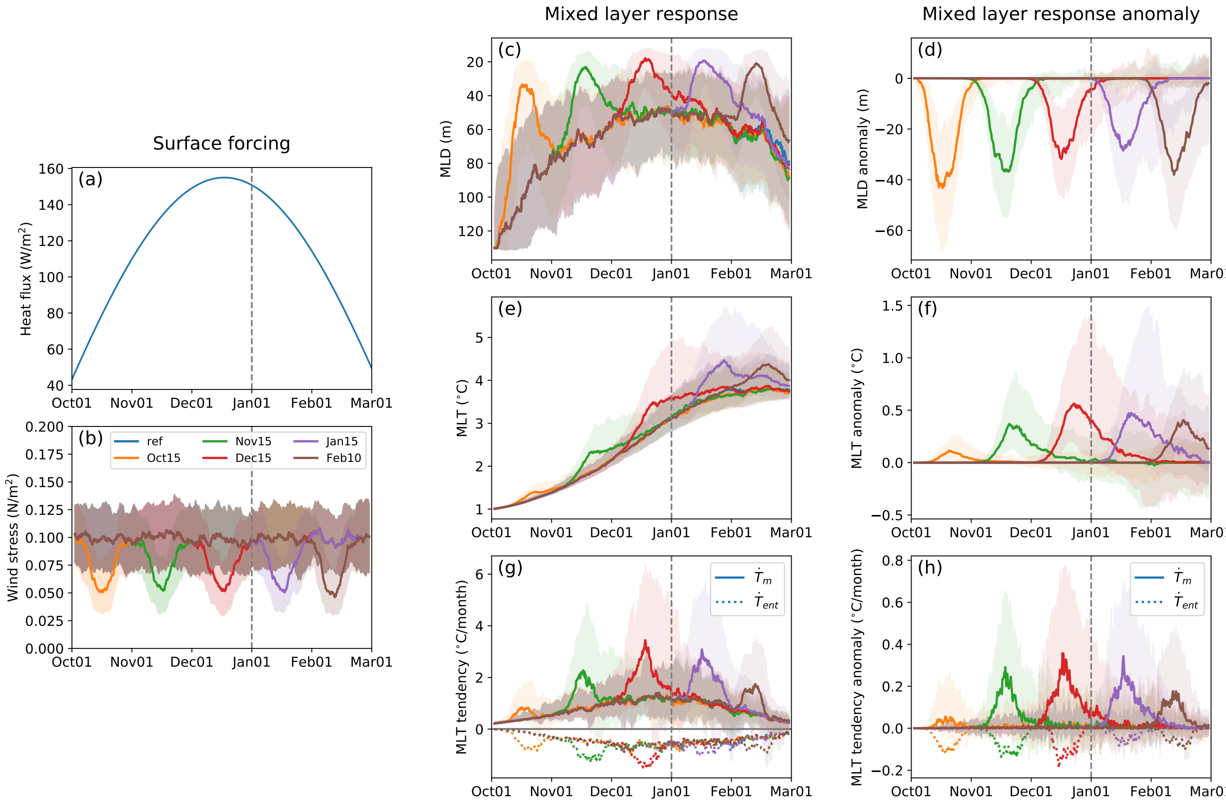

FIG. 6. Results from the idealized 1D mixing experiments. (a) The prescribed surface heat fluxes used in all experiments. (b) The synthetically generated surface wind stress used in the reference and perturbation experiments, where for the latter set a Gaussian filter was used to dampen the winds by a maximum of 50% over five different periods. Middle column shows the MLD (c), MLT (e) and MLT tendency (g) responses. The right column (d, f, h) shows the mixed layer response anomalies relative to the reference case with no wind perturbation. Each experiment consists of 200 ensemble members forced by a unique wind time series constructed from a red noise spectrum. The shading represents the interquartile range, and solid lines represent the median response. In (g, h), dotted lines represent mixed layer temperature tendency associated with entrainment $\dot{T}_{ent}$. The interquartile range for $\dot{T}_{ent}$ is omitted for clarity. See Appendix A1 for further details.

generated from a red-noise spectrum and have a time-mean magnitude of 0.1 N m^{-2}. For a single experiment, we conducted 200 simulations, each with a unique surface wind forcing.

For the reference case, the mixed layer gradually shoals and warms between October and February, reaching a minimum depth of roughly 50 m and a maximum temperature of approximately 4°C, which are consistent with observations (Figure 6). In the perturbation experiments, a Gaussian kernel is used to reduce the time-mean wind stress magnitude by a maximum value of 50% over various 10-day windows. The time-mean wind strength is reduced during the perturbation period without modifying the temporal variance.

Reducing the strength of the winds increases the rate at which the mixed layer shoals and warms. The amplitude of the MLD shoaling is not sensitive to the timing of the wind anomaly, with the median response ranging between 30–40 m. In contrast, the amplitude of mixed layer warming varies substantially with the timing of the wind perturbation. The median MLT anomaly ranges from 0.1 °C when the wind perturbation is applied in mid-October to 0.5 °C when the winds are reduced by an equivalent amount in mid-December. The latter warming anomaly occurs when the MLD and surface heat fluxes are at their respective minimum and maximum.

In the perturbation experiments, weaker winds lead to an increase in entrainment-driven mixed layer cooling $\dot{T}_{ent}$, which is consistent with what is inferred from observations in late 2016 and 2019 (Figure 4). However, the simulated response of $\dot{T}_{ent}$ is sensitive to the temporal variance of the surface winds. In experiments where the temporal variance is reduced in a similar manner as the temporal mean, the change in $\dot{T}_{ent}$ is negligible (not shown). These results indicate that wind-driven entrainment is strongly controlled by the temporal variance of the wind stress amplitude, with high-wind extremes having a disproportionate impact on entrainment.

Additional simulations (not shown here) were conducted to evaluate the sensitivity of the mixed layer responses to the duration and sign of the wind perturbation. Prolonging the weakening of the winds leads to equivalent changes in the MLD and heating tendency anomalies, with the extended accumulation of $\dot{T}$ anomalies resulting in a larger absolute change in MLT. Applying a positive wind perturbation produces a response opposite to the case with weaker winds, albeit with more minor MLT anomalies due to the deeper mixed layers.

Though idealized, these numerical simulations demonstrate that a reduction in wind-driven mixing can generate MLT anomalies similar in magnitude to those observed during the austral spring and summer of 2016/2017 and 2019/2020. The decrease in northward Ekman transport, a process not included in our idealized model, would further augment the surface warming response.

e. Role of internal climate variability

Given the rarity of these abrupt circumpolar warming events and our short observational record, we examine output from the 40-member CESM1-LE to gain a more robust understanding of

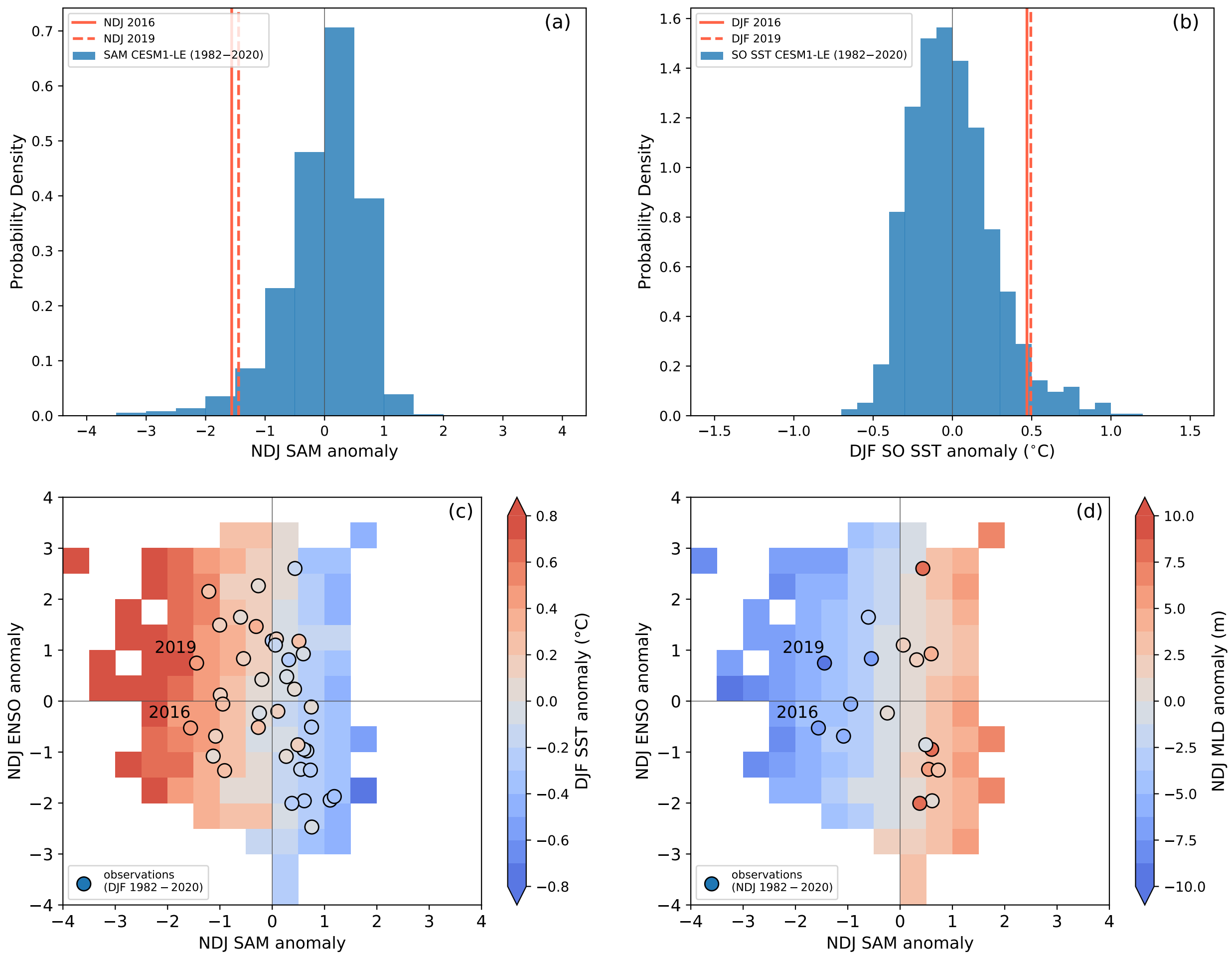

FIG. 7. Comparisons of SAM and Southern Ocean SST variability in the 40-member CESM1-LE with observations during 1982–2020. (a) Probability density distribution of the November–January (NDJ) SAM index in the CESM1-LE. (b) As in (a), but for domain-averaged DJF Southern Ocean SST anomalies across 50°–65°S. (c) Composites of domain-averaged DJF Southern Ocean SST anomalies in relation to NDJ SAM and ENSO. (d) As in (c), but showing NDJ Southern MLD anomalies. For the CESM1-LE results, anomalies refer to deviations from the ensemble mean. In (a) and (b), the frequency distributions of SAM and Southern Ocean SST are generated using 0.5 standard deviations and 0.1°C bins, respectively. For the observed seasonal averages shown here, the listed year represents the year the season begins.

these phenomena. Specifically, we investigate the response of summertime Southern Ocean SST (December–February; DJF) to variations of SAM in the preceding austral spring. An observational analysis of the lead-lag relationship between the SAM index and DJF SST across 50°–65°S shows that maximal correlation ($r \approx -0.75$) is attained when SST is lagged by one month. Therefore, we assess the relationship between Southern Ocean SST anomalies in DJF with SAM variability in November–January (NDJ) in the CESM1-LE. To isolate the effect of internal variability, we evaluate the variance of SAM and Southern Ocean SST after removing the ensemble-mean values, which represent the responses to anthropogenic forcing.

Though rare, Southern Ocean climate extremes like those observed in late 2016 and 2019 appear in the CESM1-LE (Figure 7a,b). In the CESM1-LE, NDJ periods where the SAM index is more than 1.5 standard deviations below average occur roughly once every 20 years. The distribution of NDJ SAM events also has a notable skew towards negative SAM events (Figure 7a). Importantly, the simulated Southern Ocean SST and MLD responses to late-spring SAM variability are consistent with observations. In particular, the mixed layer warming and shoaling observed in late 2016 and 2019 are consistent with equivalent events in the CESM1-LE (Figure 7c, d). To quantify the relative effect of SAM and ENSO in the CESM1-LE, we create composites of Southern Ocean SST and MLD anomalies using 0.5 standard deviation bins. In the CESM1-LE, strong SAM and ENSO events can occur independently, and it is evident that SAM has the dominant control over domain-averaged SST and MLD anomalies across 50°S–65°S. The sensitivity of summertime Southern Ocean SST and MLD to SAM variability is less apparent for individual ensemble members, and a strong dependence on SAM only emerges after averaging anomalies across the 40-member ensemble. These results indicate that other modes of variability significantly impact interannual variations of Southern Ocean SST and MLD in austral spring.

4. Discussion

This study demonstrates that the relative seasonal phasing of MLD shoaling and air-sea heat fluxes is a key driver of interannual variability in summertime Southern Ocean SST. Between September and December, the zonally averaged MLD between 50°S–65°S shoals from its winter maximum of ~150 m to its summer minimum of ~50 m (Fig. 5). The rate at which this shoaling occurs varies substantially from year to year and produces an equivalently large spread in the rate at which the mixed layer warms. In the austral spring of 2016 and 2019, the Southern Ocean mixed layer shoaled at the fastest rates observed during the Argo era, which amplified the warming effect of solar insolation when it was near its seasonal maximum. During both events, the anomalous MLD shoaling was initiated by a dramatic weakening of the circumpolar westerlies associated with strong negative SAM events. The weaker westerlies also reduced northward Ekman transport, further amplifying the mixed layer warming.

While several studies have shown that SAM has substantial control over springtime MLD and MLT (e.g., Sen Gupta and England 2006; Sallée et al. 2010), this study quantifies the high degree to which mixed layer warming is sensitive to the timing of the SAM anomalies. In particular, a sustained negative SAM event in November is expected to yield surface warming anomalies that are at least twice that produced by a similar SAM event occurring one month earlier. The late 2016 and 2019 warming events followed intense periods of negative SAM, which peaked during November and December, during which the MLT response to surface wind variability was maximal. This temporal sensitivity may explain why the negative SAM event in late 2002 did not lead to anomalous surface warming as severe as what was observed in late 2016 and 2019 (Figs. 1a, 2c). Though the late 2002 negative SAM event was just as intense and more prolonged than the 2016 and 2019 SAM events, the former peaked in October before transitioning to a more neutral state in November.

Abrupt circumpolar surface warming events, such as those observed across the Southern Ocean in late 2016 and 2019, occur in the CESM1-LE. These events are relatively rare, occurring roughly every 20 years in the CESM1-LE. Additionally, the Southern Ocean SST and MLD response to SAM in the CESM1-LE aligns well with recent observations. The CESM1-LE also features springtime negative SAM events that are more extreme than what has been observed over the past four decades, which suggests that the SAM variability may drive even more intense summertime surface warming anomalies in the future. In the CESM1-LE, SAM has a much stronger influence on zonally averaged summertime SST variability across the circumpolar channel than ENSO. However, examining individual ensemble members reveals that ENSO and other modes of variability can substantially modulate summertime Southern Ocean SST variability in a given year. Nevertheless, we conclude that the anomalous circumpolar warming of late 2016 and 2019 were primarily manifestations of internal climate variability. This assessment is in agreement with previous analyses that examine mechanisms responsible for recent declines in Antarctic SIE (e.g., Stuecker et al. 2017; Eayrs et al. 2021).

Given the spatial extent, timescale, and magnitude of the late 2016 and 2019 circumpolar surface warming anomalies, it is unlikely that these events signify a long-term shift in the South

Ocean climate. As the circumpolar westerlies continue to intensify and shift poleward, the upper overturning cell of the Southern Ocean is expected to strengthen, increasing the upwelling of warm Circumpolar Deep Water across the Antarctic sea ice zone (Ferreira et al. 2015; Kostov et al. 2017). Additionally, stronger winds will likely energize eddies across the circumpolar channel that will partially negate the Ekman overturning response (Farneti et al. 2010; Doddridge et al. 2019). However, the warming rates associated with these adjustments to the Southern Ocean overturning circulation are expected to be orders of magnitude smaller than the anomalous surface warming observed during the austral spring of 2016 and 2019. Further, the recent circumpolar surface warming events spanned the ice-free regions of the Southern Ocean, where potential temperature decreases with depth below the seasonal pycnocline. However, there is evidence that interannual upper ocean upwelling trends contributed substantially to the prolonged period of below-average Antarctic SIE between 2016 and 2020 Meehl et al. (2019). The recent decline in Antarctic sea ice cover has been most pronounced in the Weddell Sea (Parkinson 2019), which featured large open-ocean polynyas and deep convection during the winters of 2016 and 2017 (Cheon and Gordon 2019). These polynya events were facilitated by enhanced upwelling across the Weddell Gyre, which gradually eroded the local pycnocline and preconditioned the region for deep convection (Campbell et al. 2019). Thus, we surmise that the anomalous Southern Ocean surface warming and sea ice loss since 2016 were primarily due to a culmination of several climate processes acting over sub-seasonal to interannual timescales.

Additional work is needed to determine how the variability of SAM and its impacts on Southern Ocean MLD and SST will evolve under anthropogenic forcing. Previous studies have primarily focused on the mean-state ocean response to the ongoing trend toward a more positive SAM phase, in particular, the ocean overturning response to a strengthening and poleward shift of the circumpolar westerlies (e.g., Bitz and Polvani 2012; Ferreira et al. 2015; Kostov et al. 2017). However, our results demonstrate that near-surface processes acting on sub-seasonal timescales will set future surface warming extremes. The current positive trend in the SAM index is largest in austral summer (Fogt and Marshall 2020), which favors more vigorous wind-driven mixing and deeper mixed layers. On the other hand, current surface warming and freshening trends will induce stronger near-surface stratification and possibly shallower mixed layers. Over the past several decades, these competing processes have led to a deepening of the Southern Ocean mixed layer and a concurrent enhancement of the stratification across the base of the mixed layer (Sallée et al. 2021). The extent to which these trends persist will impact the frequency and intensity of future abrupt surface warming events and marine heatwaves in the Southern Ocean.

5. Conclusions

The abrupt Southern Ocean surface warming anomalies of late 2016 and 2019 were primarily the result of amplified air-sea heating and reduced northward Ekman transport. The former effect was due to an unusually early springtime shoaling of the Southern Ocean mixed layer. Both surface warming events were initiated by a collapse of the circumpolar westerlies associated with extreme negative SAM events. Equivalent warming events are found in the CESM1-LE, wherein the Southern Ocean SST and MLD response to SAM are consistent with recent observations. Therefore, it is plausible that recent Southern Ocean surface warming anomalies are purely the result of internal variability. Generalizing these recent circumpolar surface warming events, we show that interannual variability of summertime Southern Ocean SST is controlled by the variability of SAM in austral spring. Further, the amplitude of these warming events is modulated by the mean-state MLD, whereby deeper mixed layers favor more muted SST variability.

As the Southern Ocean climate evolves over the 21st century, the frequency and intensity of surface warming extremes will depend on the evolution of SAM, surface winds, and MLD. Though past studies have shown the current trend towards positive SAM will eventually lead to sustained surface warming across the Southern Ocean (Ferreira et al. 2015; Bitz and Polvani 2012), it is less clear how the interannual variability of SAM and summertime Southern Ocean SST will co-evolve. The Southern Ocean MLD is a critical bridge that links future Southern Ocean warming across decadal and interannual timescales, with shallower time-mean MLDs facilitating more extreme variations in SST. Projecting the evolution of Southern Ocean MLD is complicated by its dependence on competing processes: the projected strengthening of the circumpolar westerlies and increases in surface buoyancy fluxes via warming and enhanced freshwater fluxes (Meredith et al. 2019; Sallée et al. 2021). In a scenario where stronger winds dominate MLD trends, the Southern Ocean surface may experience steady decadal warming but reduced interannual variability due to a concurrent deepening of the mixed layer in spring and summer. Alternatively, if the surface mixed layer shoals over the coming decades, the region will likely experience more intense surface warming extremes, which would exacerbate the impact of the expected time-mean surface warming trend. These extreme warming scenarios will have profound consequences for the viability of regional ecosystems and biogeochemical processes. Thus, it is critical to establish bounds on the temporal variance that may envelope future warming trends.

Acknowledgments. E.A.W. acknowledges support from Caltech's Terrestrial Hazard Observations and Reporting Center. D.B.B. was supported by the National Science Foundation Graduate Research Fellowship Program (NSF Grant DGE-1745301). A.F.T. received support from NSF award OCE-1756956 and the Internal Research and Technology Development program (Earth 2050), Jet Propulsion Laboratory, California Institute of Technology. E.A.W. and S.C.R. received support through the SOCCOM Project, funded by the National Science Foundation, Division of Polar Programs (NSF PLR-1425989 and OPP-1936222). E.A.W. and S.C.R. also received funding from NOAA as part of the US Argo Program via grant NA20OAR4320271 to the University of Washington.

Data availability statement. All data and reanalysis products used in this study are sourced from publicly accessible repositories. NOAA Optimum Interpolation SST V2 data were retrieved from `https://psl.noaa.gov/data/gridded/data.noaa.oisst.v2.html`. The Roemmich-Gilson Argo product was downloaded from `https://sio-argo.ucsd.edu/RG_Climatology.html`. ERA5 reanalysis can be accessed at `https:doi.org/10.24381/cds.f17050d7`. Model output from the CESM1-LE can be downloaded from `https://www.cesm.ucar.edu/projects/community-projects/LENS/data-sets.html`. NOAA/NSIDC Climate Data Record of Passive Microwave Sea Ice Concentration (Version 4) can be accessed at `https://doi.org/10.7265/efmz-2t65z`. Python code for carrying out analysis and generating figures is available at `https://doi.org/10.5281/zenodo.6588645`.

APPENDIX

A1. Ensemble experiments with a 1D mixing model

To evaluate the impact of wind perturbations on MLT warming, we use a modified version of the Kraus-Turner 1D upper ocean mixing model (Kraus and Turner 1967; Niiler 1975; Niiler and Kraus 1977). This bulk mixed layer model simulates the evolution of the surface mixed layer by balancing the stabilizing effect of surface buoyancy fluxes (i.e., the addition of heat or freshwater to the water column) and the destabilizing effect of wind-driven mixing. Variants of the Kraus-Turner model have been used extensively to study surface mixed layer variations over a wide range of settings, including in subpolar regions (Biddle et al. 2017). Following Chen et al. (1994), the entrainment rate, w_{ent}, of the mixed layer is given by

$$w_{ent} = \frac{P_w - P_b}{h_m \Delta b}, \tag{A1}$$

where Δb is the buoyancy difference across the base of the mixed layer, and P_w and P_b are work provided by surface wind stress and the potential energy supplied by surface buoyancy fluxes, respectively. P_w and P_b are given by

$$P_w = 2\gamma_1 u_*^3, \tag{A2}$$

$$P_b = \frac{h_m}{2} \left[(1+\gamma_2) B_0 - (1-\gamma_2) |B_0| \right], \tag{A3}$$

where $\gamma_1 = 0.4$ and $\gamma_2 = 0.18$ are empirically derived mixing coefficients, u_* is the friction velocity, and B_0 is the total surface buoyancy flux. The above formulation is valid for a stably stratified water column ($\Delta b > 0$). For scenarios where $P_w - P_b > 0$, the mixed layer deepens and (A1) is used to determine the entrainment rate. For cases of mixed layer shoaling, we assume P_w and P_b are in balance and we use the relationships (A2) and (A3) to determine h_m.

The mixing model is initialized with idealized temperature and salinity profiles representative of the circumpolar channel between 50°–65°S in early October. At the start of each simulation, the mixed layer depth is set to 125 m, and temperature and salinity in the mixed layer are set to 1 °C and 33.4 PSU, respectively. Below the mixed layer, there is a 150 m thick seasonal pycnocline, across which temperature and salinity linearly transition to fixed values of 0°C and ~33.6 PSU, respectively. We prescribe a surface heat flux that approximates the climatological net surface heating across the circumpolar channel between October and March (150 days total). To isolate the impact of surface winds and heating, we impose a constant surface freshwater flux (i.e., precipitation minus evaporation) of 1 mm day^{-1}. The buoyancy forcing is combined with a synthetically generated surface wind stress τ, which is modeled as the sum of a red-noise sequence $\hat{\tau}(t)$ and a mean offset $\overline{\tau}$:

$$\tau(t) = \hat{\tau}(t) + \overline{\tau}, \tag{A4}$$

$$\hat{\tau}(t) = a\,\hat{\tau}(t - \Delta t) + \sqrt{(1 - a^2)}\,\epsilon(t), \tag{A5}$$

where $a = 0.9$ is the lag-1 auto-correlation coefficient, $\Delta t = 6$ hours is the time step, ϵ is a randomly generated white noise sequence with a standard deviation of 0.05, and $\overline{\tau}$ = 0.1 N m^{-2}. The numerical model is evolved with a vertical resolution of 0.25 m and a 6 hourly time step. A total of six ensemble experiments are carried out: one control experiment consisting of 200 independent simulations, each with a unique wind forcing, and five perturbation experiments wherein $\overline{\tau}$ is reduced over different time windows, centered on days 15, 45, 75, 105, and 135 days (after October 1). For the perturbation experiments, the magnitude of the time-mean wind stress is reduced by a maximum of 50% using a Gaussian window with a standard deviation of 5 days. By perturbing $\overline{\tau}$ in Equation (A5), the temporal variance of τ is preserved.

References

Armour, K. C., J. Marshall, J. R. Scott, A. Donohoe, and E. R. Newsom, 2016: Southern Ocean warming delayed by circumpolar upwelling and equatorward transport. *Nature Geoscience*, **9 (7)**, 549–554, https://doi.org/10.1038/ngeo2731.

Biddle, L. C., K. J. Heywood, J. Kaiser, and A. Jenkins, 2017: Glacial meltwater identification in the Amundsen Sea. *Journal of Physical Oceanography*, JPO–D–16–0221.1, https://doi.org/10.1175/JPO-D-16-0221.1.

Bintanja, R., G. J. V. Oldenborgh, S. S. Drijfhout, B. Wouters, and C. A. Katsman, 2013: Important role for ocean warming and increased ice-shelf melt in Antarctic sea-ice expansion. *Nature Geoscience*, **6 (5)**, 376–379, https://doi.org/10.1038/ngeo1767.

Bitz, C. M., and L. M. Polvani, 2012: Antarctic climate response to stratospheric ozone depletion in a fine resolution ocean climate model. *Geophysical Research Letters*, **39 (20)**, https://doi.org/10.1029/2012GL053393.

Campbell, E. C., E. A. Wilson, G. W. Moore, S. C. Riser, C. E. Brayton, M. R. Mazloff, and L. D. Talley, 2019: Antarctic offshore polynyas linked to Southern Hemisphere climate anomalies. *Nature*, **570 (7761)**, 319–325, https://doi.org/10.1038/s41586-019-1294-0.

Carranza, M. M., and S. T. Gille, 2015: Southern Ocean wind-driven entrainment enhances satellite chlorophyll-a through the summer. *Journal of Geophysical Research: Oceans*, **120 (1)**, 304–323, https://doi.org/10.1002/2014JC010203.

Cavalieri, D. J., C. L. Parkinson, and K. Y. Vinnikov, 2003: 30-year satellite record reveals contrasting Arctic and Antarctic decadal sea ice variability. *Geophysical Research Letters*, **30 (18)**, https://doi.org/10.1029/2003GL018031.

Chen, D., L. M. Rothstein, and A. J. Busalacchi, 1994: A Hybrid Vertical Mixing Scheme and Its Application to Tropical Ocean Models. *Journal of Physical Oceanography*, **24 (10)**, 2156–2179, https://doi.org/10.1175/1520-0485(1994)024<2156:AHVMSA>2.0.CO;2.

Cheon, W. G., and A. L. Gordon, 2019: Open-ocean polynyas and deep convection in the Southern Ocean. *Scientific Reports*, **9 (1)**, 6935, https://doi.org/10.1038/s41598-019-43466-2.

Chung, E.-S., and Coauthors, 2022: Antarctic sea-ice expansion and Southern Ocean cooling linked to tropical variability. *Nature Climate Change*, https://doi.org/10.1038/s41558-022-01339-z.

Ciasto, L. M., and M. H. England, 2011: Observed ENSO teleconnections to Southern Ocean SST anomalies diagnosed from a surface mixed layer heat budget. *Geophysical Research Letters*, **38 (9)**, https://doi.org/10.1029/2011GL046895.

de Boyer Montégut, C., G. Madec, A. S. Fischer, A. Lazar, and D. Iudicone, 2004: Mixed layer depth over the global ocean: An examination of profile data and a profile-based climatology. *Journal of Geophysical Research C: Oceans*, **109 (12)**, 1–20, https://doi.org/10.1029/2004JC002378.

Ding, Q., E. J. Steig, D. S. Battisti, and J. M. Wallace, 2012: Influence of the tropics on the southern annular mode. *Journal of Climate*, **25 (18)**, 6330–6348, https://doi.org/10.1175/JCLI-D-11-00523.1.

Doddridge, E. W., J. Marshall, H. Song, J. M. Campin, M. Kelley, and L. Nazarenko, 2019: Eddy Compensation Dampens Southern Ocean Sea Surface Temperature Response to Westerly Wind Trends. *Geophysical Research Letters*, **46 (8)**, 4365–4377, https://doi.org/10.1029/2019GL082758.

Dong, S., S. T. Gille, and J. Sprintall, 2007: An assessment of the Southern Ocean mixed layer heat budget. *Journal of Climate*, **20 (17)**, 4425–4442, https://doi.org/10.1175/JCLI4259.1.

Dong, S., J. Sprintall, S. T. Gille, and L. Talley, 2008: Southern ocean mixed-layer depth from Argo float profiles. *Journal of Geophysical Research: Oceans*, **113 (6)**, https://doi.org/10.1029/2006JC004051.

du Plessis, M., S. Swart, L. C. Biddle, I. S. Giddy, P. M. S. Monteiro, C. J. C. Reason, A. F. Thompson, and S. Nicholson, 2022: The Daily-Resolved Southern Ocean Mixed Layer: Regional Contrasts Assessed Using Glider Observations. *Journal of Geophysical Research: Oceans*, **127 (4)**, https://doi.org/10.1029/2021JC017760.

Eayrs, C., X. Li, M. N. Raphael, and D. M. Holland, 2021: Rapid decline in Antarctic sea ice in recent years hints at future change. *Nature Geoscience*, **14 (7)**, 460–464, https://doi.org/10.1038/s41561-021-00768-3.

Fan, T., C. Deser, and D. P. Schneider, 2014: Recent Antarctic sea ice trends in the context of Southern Ocean surface climate variations since 1950. *Geophysical Research Letters*, **41 (7)**, 2419–2426, https://doi.org/10.1002/2014GL059239.

Farneti, R., T. L. Delworth, A. J. Rosati, S. M. Griffies, and F. Zeng, 2010: The role of mesoscale eddies in the rectification of the Southern ocean response to climate change. *Journal of Physical Oceanography*, **40 (7)**, 1539–1557, https://doi.org/10.1175/2010JPO4353.1.

Ferreira, D., J. Marshall, C. M. Bitz, S. Solomon, and A. Plumb, 2015: Antarctic ocean and sea ice response to ozone depletion: A two-time-scale problem. *Journal of Climate*, **28 (3)**, 1206–1226, https://doi.org/10.1175/JCLI-D-14-00313.1.

Fogt, R. L., and G. J. Marshall, 2020: The Southern Annular Mode: Variability, trends, and climate impacts across the Southern Hemisphere. *WIREs Climate Change*, **11 (4)**, https://doi.org/10.1002/wcc.652.

Frölicher, T. L., E. M. Fischer, and N. Gruber, 2018: Marine heatwaves under global warming. *Nature*, **560 (7718)**, 360–364, https://doi.org/10.1038/s41586-018-0383-9.

Gao, Y., I. Kamenkovich, N. Perlin, and B. Kirtman, 2022: Oceanic Advection Controls Mesoscale Mixed Layer Heat Budget and Air–Sea Heat Exchange in the Southern Ocean. *Journal of Physical Oceanography*, **52 (4)**, 537–555, https://doi.org/10.1175/JPO-D-21-0063.1.

Haumann, F. A., N. Gruber, and M. Münnich, 2020: Sea-Ice Induced Southern Ocean Subsurface Warming and Surface Cooling in a Warming Climate. *AGU Advances*, **1 (2)**, https://doi.org/10.1029/2019AV000132.

Hersbach, H., and Coauthors, 2020: The ERA5 global reanalysis. *Quarterly Journal of the Royal Meteorological Society*, **146 (730)**, 1999–2049, https://doi.org/10.1002/qj.3803.

Hobday, A. J., and Coauthors, 2016: A hierarchical approach to defining marine heatwaves. *Progress in Oceanography*, **141**, 227–238, https://doi.org/10.1016/j.pocean.2015.12.014.

Holbrook, N. J., and Coauthors, 2019: A global assessment of marine heatwaves and their drivers. *Nature Communications*, **10 (1)**, 2624, https://doi.org/10.1038/s41467-019-10206-z.

Kay, J. E., and Coauthors, 2015: The Community Earth System Model (CESM) Large Ensemble Project: A Community Resource for Studying Climate Change in the Presence of Internal Climate Variability. *Bulletin of the American Meteorological Society*, **96 (8)**, 1333–1349, https://doi.org/10.1175/BAMS-D-13-00255.1.

Kostov, Y., J. Marshall, U. Hausmann, K. C. Armour, D. Ferreira, and M. M. Holland, 2017: Fast and slow responses of Southern Ocean sea surface temperature to SAM in coupled climate models. *Climate Dynamics*, **48 (5-6)**, 1595–1609, https://doi.org/10.1007/s00382-016-3162-z.

Kraus, E. B., and J. S. Turner, 1967: A one-dimensional model of the seasonal thermocline II. The general theory and its consequences. *Tellus*, **19 (1)**, 98–106, https://doi.org/10.3402/tellusa.v19i1.9753.

Li, X., and Coauthors, 2021: Tropical teleconnection impacts on Antarctic climate changes. *Nature Reviews Earth & Environment*, **2 (10)**, 680–698, https://doi.org/10.1038/s43017-021-00204-5.

Marshall, G. J., 2003: Trends in the Southern Annular Mode from observations and reanalyses. *Journal of Climate*, **16 (24)**, 4134–4143, https://doi.org/10.1175/1520-0442(2003)016<4134:TITSAM>2.0.CO;2.

Meehl, G. A., J. M. Arblaster, C. M. Bitz, C. T. Y. Chung, and H. Teng, 2016: Antarctic sea-ice expansion between 2000 and 2014 driven by tropical Pacific decadal climate variability. *Nature Geoscience*, **9 (8)**, 590–595, https://doi.org/10.1038/ngeo2751.

Meehl, G. A., J. M. Arblaster, C. T. Y. Chung, M. M. Holland, A. DuVivier, L. A. Thompson, D. Yang, and C. M. Bitz, 2019: Sustained ocean changes contributed to sudden Antarctic sea ice retreat in late 2016. *Nature Communications*, **10 (1)**, https://doi.org/10.1038/s41467-018-07865-9.

Meier, W., F. Fetterer, M. Savoie, S. Mallory, R. Duerr, and J. Stroeve, 2013: NOAA/NSIDC Climate Data Record of Passive Microwave Sea Ice Concentration. NSIDC: National Snow and Ice Data Center, https://doi.org/10.7265/N59P2ZTG.

Meredith, M., and Coauthors, 2019: Polar Regions. *Ocean Cryosph. a Chang. Clim.*, H.-O. Pörtner, D. C. Roberts, V. Masson-Delmotte, P. Zhai, M. Tignor, E. Poloczanska, K. Mintenbeck, A. Alegría, M. Nicolai, A. Okem, J. Petzold, B. Rama, and N. M. Weyer, Eds., Cambridge University Press, Cambridge, chap. 3, 203–320, https://doi.org/10.1017/9781009157964.005.

Niiler, P. P., 1975: The deepening of the wind-mixed layer. *Journal of Marine Research*, **33 (3)**, 405–422.

Niiler, P. P., and E. B. Kraus, 1977: One Dimensional Models of the Upper Ocean. Pergamon, 143–172 pp.

Oliver, E. C. J., J. A. Benthuysen, S. Darmaraki, M. G. Donat, A. J. Hobday, N. J. Holbrook, R. W. Schlegel, and A. S. Gupta, 2021: Marine Heatwaves. *Annual Review of Marine Science*, **13 (1)**, 313–342, https://doi.org/10.1146/annurev-marine-032720-095144.

Parkinson, C. L., 2019: A 40-y record reveals gradual Antarctic sea ice increases followed by decreases at rates far exceeding the rates seen in the Arctic. *Proceedings of the National Academy of Sciences*, **116 (29)**, 14 414–14 423, https://doi.org/10.1073/pnas.1906556116.

Pellichero, V., J. B. Sallée, S. Schmidtko, F. Roquet, and J. B. Charrassin, 2017: The ocean mixed layer under Southern Ocean sea-ice: Seasonal cycle and forcing. *Journal of Geophysical Research: Oceans*, **122 (2)**, 1608–1633, https://doi.org/10.1002/2016JC011970.

Purich, A., and M. H. England, 2019: Tropical Teleconnections to Antarctic Sea Ice During Austral Spring 2016 in Coupled Pacemaker Experiments. *Geophysical Research Letters*, **46 (12)**, 6848–6858, https://doi.org/10.1029/2019GL082671.

Purich, A., M. H. England, W. Cai, A. Sullivan, and P. J. Durack, 2018: Impacts of broad-scale surface freshening of the Southern Ocean in a coupled climate model. *Journal of Climate*, **31 (7)**, 2613–2632, https://doi.org/10.1175/JCLI-D-17-0092.1.

Rackow, T., S. Danilov, H. F. Goessling, H. H. Hellmer, D. V. Sein, T. Semmler, D. Sidorenko, and T. Jung, 2022: Delayed Antarctic sea-ice decline in high-resolution climate change simulations. *Nature Communications*, **13 (1)**, 637, https://doi.org/10.1038/s41467-022-28259-y.

Reynolds, R. W., N. A. Rayner, T. M. Smith, D. C. Stokes, and W. Wang, 2002: An improved in situ and satellite SST analysis for climate. *Journal of Climate*, **15 (13)**, 1609–1625, https://doi.org/10.1175/1520-0442(2002)015<1609:AIISAS>2.0.CO;2.

Roemmich, D., and J. Gilson, 2009: The 2004-2008 mean and annual cycle of temperature, salinity, and steric height in the global ocean from the Argo Program. *Progress in Oceanography*, **82 (2)**, 81–100, https://doi.org/10.1016/j.pocean.2009.03.004.

Sallée, J. B., K. G. Speer, and S. R. Rintoul, 2010: Zonally asymmetric response of the Southern Ocean mixed-layer depth to the Southern Annular Mode. *Nature Geoscience*, **3 (4)**, 273–279, https://doi.org/10.1038/ngeo812.

Sallée, J.-B., and Coauthors, 2021: Summertime increases in upper-ocean stratification and mixed-layer depth. *Nature*, **591 (7851)**, 592–598, https://doi.org/10.1038/s41586-021-03303-x.

Schlosser, E., F. A. Haumann, and M. N. Raphael, 2018: Atmospheric influences on the anomalous 2016 Antarctic sea ice decay. *Cryosphere*, **12 (3)**, 1103–1119, https://doi.org/10.5194/tc-12-1103-2018.

Sen Gupta, A., and M. H. England, 2006: Coupled ocean-atmosphere-ice response to variations in the southern annular mode. *J. Clim.*, **19 (18)**, 4457–4486, https://doi.org/10.1175/JCLI3843.1.

Simmonds, I., 2015: Comparing and contrasting the behaviour of Arctic and Antarctic sea ice over the 35 year period 1979-2013. *Annals of Glaciology*, **56 (69)**, 18–28, https://doi.org/10.3189/2015AoG69A909.

Smale, D. A., and Coauthors, 2019: Marine heatwaves threaten global biodiversity and the provision of ecosystem services. *Nature Climate Change*, **9 (4)**, 306–312, https://doi.org/10.1038/s41558-019-0412-1.

Stuecker, M. F., C. M. Bitz, and K. C. Armour, 2017: Conditions leading to the unprecedented low Antarctic sea ice extent during the 2016 austral spring season. *Geophysical Research Letters*, **44 (17)**, 9008–9019, https://doi.org/10.1002/2017GL074691.

Tamsitt, V., L. D. Talley, M. R. Mazloff, and I. Cerovecki, 2016: Zonal variations in the Southern Ocean heat budget. *Journal of Climate*, **29 (18)**, 6563–6579, https://doi.org/10.1175/JCLI-D-15-0630.1.

Turner, J., T. Phillips, G. J. Marshall, J. S. Hosking, J. O. Pope, T. J. Bracegirdle, and P. Deb, 2017: Unprecedented springtime retreat of Antarctic sea ice in 2016. *Geophysical Research Letters*, **44 (13)**, 6868–6875, https://doi.org/10.1002/2017GL073656.

Wang, G., H. H. Hendon, J. M. Arblaster, E. P. Lim, S. Abhik, and P. van Rensch, 2019: Compounding tropical and stratospheric forcing of the record low Antarctic sea-ice in 2016. *Nature Communications*, **10 (1)**, 13, https://doi.org/10.1038/s41467-018-07689-7.

Yuan, X., and D. G. Martinson, 2000: Antarctic sea ice extent variability and its global connectivity. *Journal of Climate*, **13 (10)**, 1697–1717, https://doi.org/10.1175/1520-0442(2000)013<1697:ASIEVA>2.0.CO;2.

Zhang, L., T. L. Delworth, W. Cooke, and X. Yang, 2019: Natural variability of Southern Ocean convection as a driver of observed climate trends. *Nature Climate Change*, **9 (1)**, 59–65, https://doi.org/10.1038/s41558-018-0350-3.